Dual-Polarized MIMO Antenna System for 5G Indoor base Station Applications

Loya Surendra (surendra.loya2007@gmail.com)
Koneru Lakshmaiah Education Foundation
Habihulla khan
Koneru Lakshmaiah Education Foundation

Research Article

Keywords: 5G, MIMO, CMA, 3.5 GHz, ECC, Dual-Polarization, sub-6

Posted Date: June 10th, 2022

DOI: https://doi.org/10.21203/rs.3.rs-1741223/v1

Dual-Polarized MIMO Antenna System for 5G Indoor base Station Applications

Loya Surendra[1]
KL (Deemed to be University)
Guntur, India
Usha Rama College of Engineering and Technology
Vijayawada, India
Surendra.loya2007@gmail.com

Habihulla khan[2]
KL (Deemed to be University)
Guntur, India,
habibulla@kluniversity.in

***Abstract*—In this paper a dual-polarized multiple-input multiple-output (MIMO) antenna system for fifth-generation (5G) indoor base station applications resonating at 3.5 GHz has been proposed. The initial design is a conventional patch antenna, and characteristic mode analysis (CMA) is used to determine its dual-polarized characteristics. Both orthogonal modes are excited using the full-wave approach with a 50 Ohm dual-port coaxial feed line, and operated at 3.5 GHz. The non-contact feed method is used to improve isolation between ports. Inserting an air gap between the antenna substrate and the ground metal sheet improves gain and bandwidth. Further 2x2 MIMO antenna with 8-port is designed on low cost FR4 dielectric material with 120*120*5.17 mm^3 compact volume. The MIMO antenna's performance are examined by simulation and experimental. For the proposed MIMO, high isolation, high efficiency, and appropriate gain-level characteristics have been obtained. Furthermore, throughout the whole band of interest, the calculated total active reflection coefficient (TARC) and envelope correlation coefficient (ECC) of the antenna components are very low, indicating that the proposed multi-antenna systems are capable of enormous MIMO and diversity applications. Furthermore, the antenna avoids the use of complex feeding mechanisms such as baluns or directional couplers.**

Keywords—5G, MIMO, CMA, 3.5 GHz, ECC, Dual-Polarization, sub-6

1. INTRODUCTION

Fifth-generation (5G) communications are being deployed commercially in several regions of the world. 5G has brought about faster speeds, wider coverage, and an end to the long-awaited latency and congestion problems compared to 4G. Although sub-6GHz and millimeter wave bands are recommended for 5G, most countries initially used sub-6 bands due to network availability; e.g., 3.42-3.70 GHz, India: 3.4-3.6 GHz, Australia: 3.4-3.7 GHz, Europe: 3.4-3.8 GHz, China: 3.3-3.6 GHz, USA: 3.10-3.55 GHz and 3.7-4.2 GHz [1-2]. Indoor 5G base station antennas that cover both the new licenced sub-6 GHz bands as well as the existing 2G/3G/4G bands are in high demand. Due to the benefits of increased communication channel capacity and reduced multipath fading effect, dual-polarized antennas have become widely used in the development of wireless communication systems. Dual-polarized antennas have been widely explored and consistently developed in recent years due to these advantages and diverse requirements. Patch antennas and crossed dipole antennas are widely used to achieve dual-polarization [3]. Unidirectional radiation patterns, a high overall efficiency, and decoupled ports are all required for these antennas. Furthermore, low-problem, easy-manufacturing, and low-cost qualities are also highly valued for simple and quick antenna installation in indoor scenarios [2,4,5]

Base station antennas have attracted a lot of attention in recent decades, with many types of antennas and structures. Patch antennas, slot antennas, and cross dipole antennas are the most common antennas, with polarization diversity techniques utilizing diverse polarizations becoming increasingly prevalent for base station antennas. For base station antennas, dual polarization antennas are chosen because of their unique qualities for overcoming multipath fading and improving channel capacity such as bow-tie antennas in orthogonal orientation in [2,5,6], cross-dipoles fed with balun in [7-8], crossed elliptic-H slots in [9], two pairs of folded radiation petals in [10], two crossed bow-tie dipoles in [11]. In developing base station antennas, the ability to increase channel capacity and resist the effect of

multipath fading with polarization diversity acquired highest priority. The present evolution of 5G networks is focused on the ability to multiplex data streams in parallel with time or frequency resources via multiple input multiple output (MIMO) antenna systems [2,6,11,12]. Furthermore, the potential to increase the data throughput in 5G indoor base stations through multiple-input multiple-output (MIMO) is a widely desired feature. Multiple port antennas with highly isolated ports and independent radiation patterns with a low Envelope Correlation Coefficient (ECC) between them are required for MIMO functioning [2,4,7,12].

Isolation between ports is a crucial feature, especially when multiple-port solutions are installed in tight spaces. A decoupling element in [6, 11], a neutralizing line in [8], Slot-coupled patch antennas in [9], and X-shaped isolating in [4] are some of the approaches used to increase isolation. Furthermore, the possibility of awakening distinct orthogonal modes on a hand-held device's radiating ground plane for MIMO compatibility has piqued interest in Characteristic Modes Analysis in current applications. CMA has been applied to a number of proposed planar solutions for MIMO systems that cover a variety of bands with low coupling [4]. The antenna performances are summarized in Table 2. Most of these designs have relatively large circuit's complexity, low isolation, low efficiency and low ECC values.

A 2*2 MIMO antenna system for 3.4–3.6 GHz for sub-6, 5G indoor base station applications is discussed in this paper. The use of non-contact feed reduces mutual coupling between the antenna's ports. The isolation has been enhanced and is now less than 40 dB over the whole operating range. Four separate unidirectional radiation patterns with excellent efficiency are provided by the design. The system is fabricated on an easily available, inexpensive, and widely used FR4 substrate. The system is designed using an EM full-wave commercial software CST Studio Suite. A detailed study regarding the antenna design, non-contact feed, and other parameters of the design is presented. A prototype is fabricated to verify the simulated results. The comparison between the simulated and measured results is presented and it is found that they are in good agreement. The effects of isolation between antennas and the MIMO system are also studied. It is found that ECC and Diversity Gain (DG) for the proposed system are approx. 10 dBi. The channel capacity loss (CCL) is less than less than 0.1(bits/s/Hz) for the whole operating bandwidth. As a result, no hybrid couplers or baluns are required in this design, making it a simple to manufacture and low-cost solution suitable for use as an indoor MIMO base station antenna. The paper's novelty comes from the characteristic modes-based technique utilized to create an orthogonal mode and determine which of them contributes to port coupling. The non-contact feed is introduced to minimize mutual coupling between antenna ports.

The following is a summary of the paper's structure: The original design is described in Section 2, along with the analytical and CMA study of the antenna. In Section 3, discussed feed optimization of initial antenna with dual polarized characteristics. In Section 4, a novel non-contact feed based air-gap antenna is presented to minimize isolation, and enhancement of bandwidth and gain. In Section 5, a comparison between initial and non-contact feed air-gap antenna's performance. In Section 6 and 7, the design of 2x2 MIMO antenna and its diversity performance are presented. In Section 8, proposed antenna hardware and measurement validation analysis with simulated results. Finally, Section 9 exposes the conclusion of the paper.

2. INITIAL ANTENNA DESIGN

2.1 Analytical parameters calculation for Initial design

In this section, an initial patch antenna is designed on FR4 substrate and initial theoretical expressions are calculated by using cavity model theory [13]. The cavity model method is an approximate model, which does not radiate any power from the structure. The resonance frequency of **TM** modes for the cavity is given as:

$$(f_r)_{mnp} = \frac{1}{2\pi\sqrt{\mu\epsilon}}\sqrt{\left(\frac{m\pi}{h}\right)^2 + \left(\frac{n\pi}{L}\right)^2 + \left(\frac{p\pi}{W}\right)^2} \quad (1)$$

Where h, L, and W are the antenna's height, length, and width, respectively. The numbers m, n, and p represent the number of half-cycle field variations in the x, y, and z directions, respectively.

The rectangular antenna design parameters (L & W) are calculated theoretically at 3.5 GHz frequency by using cavity model method. The antenna design on FR4 dielectric material with $\varepsilon_r = 4.3$, $and\ \ tan\delta = 0.025$ with height h=1.6mm.

L-Parameter calculation for $TM_{010}\ mode\ (m = 0, n = 1, p = 0)$ at 3.5 GHz using equation (1).

$$(f_r)_{010} = \frac{1}{2\pi\sqrt{\mu\epsilon}}\sqrt{\left(\frac{0\pi}{h}\right)^2 + \left(\frac{1\pi}{L}\right)^2 + \left(\frac{0\pi}{W}\right)^2} = \frac{C}{2L\sqrt{\varepsilon_r}},\ \ L = \frac{c}{2(f_r)_{010}\sqrt{\varepsilon_r}} = \frac{3*10^8}{2*3.5*10^8\sqrt{4.3}} = 20.66 \text{ mm}$$

W-Parameter calculation for $TM_{001}(m = 0, n = 0, p = 1)$ at 3.5Ghz (Orthogonal mode)using equation (1)

$$(f_r)_{001} = \frac{1}{2\pi\sqrt{\mu\epsilon}}\sqrt{\left(\frac{0\pi}{h}\right)^2 + \left(\frac{0\pi}{L}\right)^2 + \left(\frac{1\pi}{W}\right)^2} = \frac{1}{2W\sqrt{\mu\epsilon}} = \frac{C}{2W\sqrt{\varepsilon_r}},\ Wp = \frac{3*10^8}{2*3.5*10^8\sqrt{4.3}} = 20.66\text{mm}$$

2.2 Characteristic Modes Analysis of initial design

The characteristics mode theory was proposed by Harrington, Garbacz, and Mautz (CMT). It's a powerful and methodical tool for constructing microwave components including antennas and filters. In recent years, the usage of characteristic mode theory has benefited a wide range of applications. The structure of electromagnetic properties is the surface current modes. To solve the characteristic modes, use the following Eigen value equation [13-16].

$$[X]\ \vec{J}_n = \lambda_n[R]\vec{J}_n \tag{2}$$

Where R and X parameters are shown real and imaginary part of the Z-matrix of the conducting substance, respectively. The current properties of the conducting body as determined:

$$\vec{J} = \sum_{n=1}^{N} \alpha_n \vec{J} \tag{3}$$

In addition, after derivation:

$$\alpha_n = \frac{\langle J_n E^i \rangle}{\langle 1 + j\lambda_n \rangle} = \frac{V_n}{1 + j\lambda_n} \tag{4}$$

The conducting Body characteristics such as Modal significance (MS) is given as: Where α_n is the modal weighting expansion factor, which indicates how important the characteristic current $\overrightarrow{J_n}$ of the conducting body is in comparison to the overall current $\vec{J}$. Modal significance (MS) is one of the conducting body's features given as:

$$MS = \left|\frac{1}{1 + j\lambda_n}\right| \tag{5}$$

And Characteristic angle (CA) are

$$\alpha = 180^o - \tan^{-1}(\lambda) \tag{6}$$

There is a significant contribution of conducting body resonance when MS is near to 1 and CA is close to 180°.

According to characteristic modes analysis, the initial rectangular antenna was moralized up to three modes using the same parameters as the Cavity Model Method, as illustrated in figure1. Figure 2 depicts the initial antenna's modal significance values, in this plot mode-1 and mode-2 are resonated at 3.5GHz, while mode 3 is a non-resonant mode. According to the maximum value of the modal significance curve, each mode's resonance can be identified. Figure 3 depicts the initial design's characteristic angle. Figures 4 and 5 show the related surface current distributions and radiation patterns. Mode-1 and mode-2 radiation patterns in broadside and orthogonal directions.

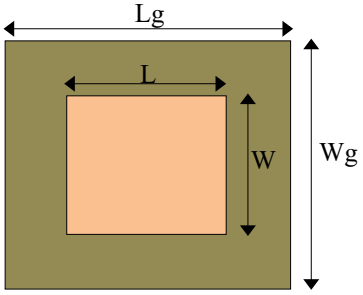

Figure 1. Initial antenna design by using CMA method

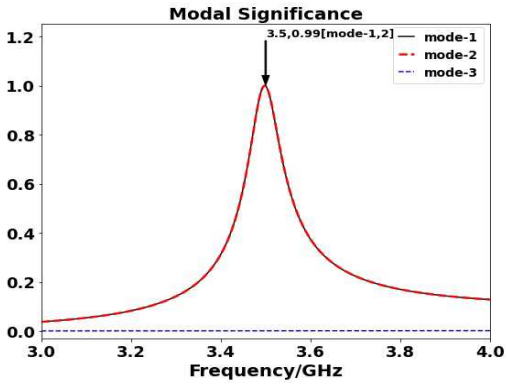

Figure 2. MS plot of initial antenna

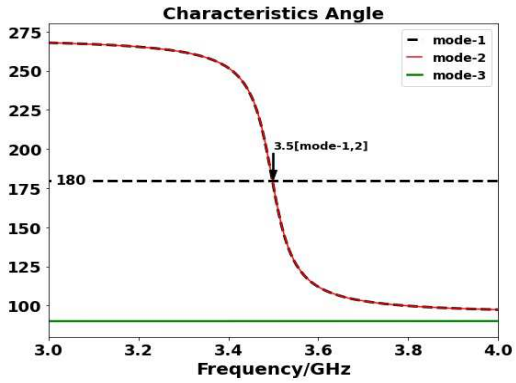

Figure 3. CA plot of initial antenna

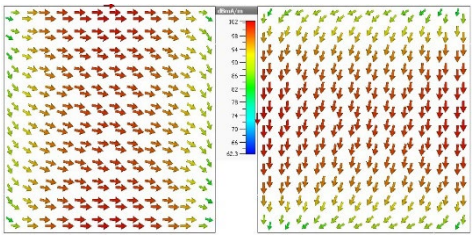

Figure 4. Surface Current Distribution of initial antenna

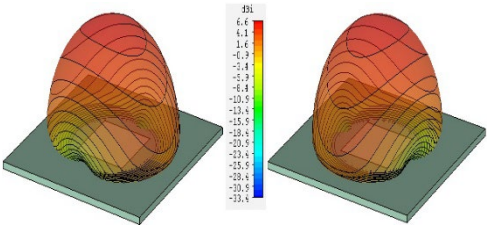

Figure 5. Radiation Pattern of initial antenna

3. FEED OPTIMIZATION OF INITIAL ANTENNA BY FULL-WAVE SIMULATION

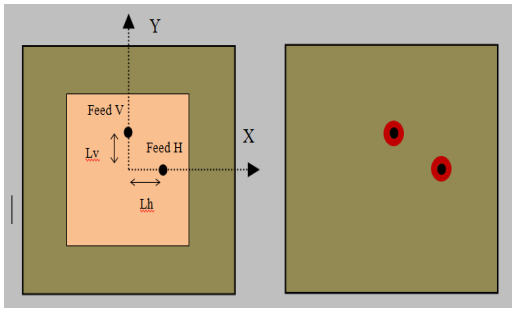

Figure 6. Initial Antenna with coaxial feeds

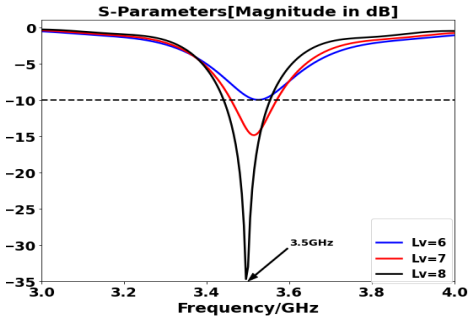

Figure 7. S11 plot of initial antenna with coaxial feeds

3.1. Feed location calculation by TLM

Figure 6 shows the initial antenna with coaxial feed and corresponding feed location (Lv) S11 plot is shown in figure 7. The location of the coaxial feed in the antenna is optimized such that the input impedance of the antenna is matched with 50 of the coaxial line impedance. The antenna is matched to the coaxial feed line at Lv = 8 mm.

The initial antenna is square (L=W), so second feed location (Lh) also have same value and same S11 plot. The below mathematics equations (7 & 8) are requires to calculation of feed location of antenna [17].

$$R_{in}(X = L_h) = R_{in}(X = \frac{L}{2})Cos^2(\frac{\pi}{L}L_h) \quad (7)$$

$$\frac{1}{R_{in}(X=\frac{L}{2})} = G_1 = \frac{1}{90}(\frac{W}{\lambda_O})^2,\ W \ll \lambda_O \quad (8)$$

Free space wavelength at 3.5GHz

$$\lambda_o = \frac{c}{f} = \frac{3 * 10^8}{3.5 * 10^9} = 85.71mm$$

Calculation of Input impedance of antenna at $(X = \frac{L}{2})$ by equation 8

$$\frac{1}{R_{in}(X = \frac{L}{2})} = G_1 = \frac{1}{90}(\frac{19.35}{85.71})^2 = 5.66 * 10^{-4}\text{Mho}$$

$$R_{in}\left(X = \frac{L}{2}\right) = 1765.80\ \Omega$$

Calculation ofL_h at 50 Ω for coaxial feed line impedance matching by equation 7

$$R_{in}(X = L_h) = 50 = 1765.80Cos^2\left(\frac{\pi}{L}L_h\right)$$

$$L_h = 8.63\ mm$$

Similar for vertical polarization feed location

$$L_v = 8.63\ mm$$

3.2. Dual polarization by dual feed

Figure 8 illustrates the S11 plot of the initial antenna with dual coaxial feeds; the red line plot depicts horizontal polarization, while the black dashed lines depict vertical polarization with respect to the feed. The direction of current for horizontal and vertical polarization is seen in the surface current in figure 9.

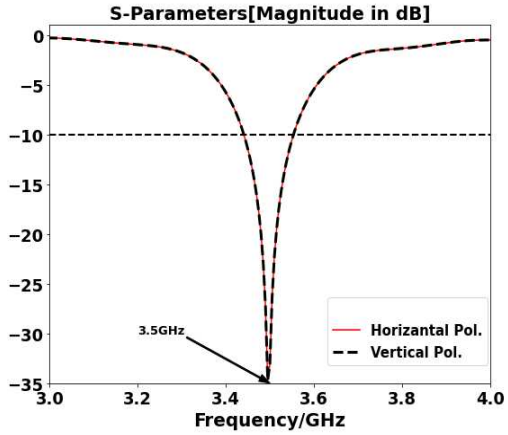

Figure 8. S11 plot of initial antenna with dual coaxial feeds

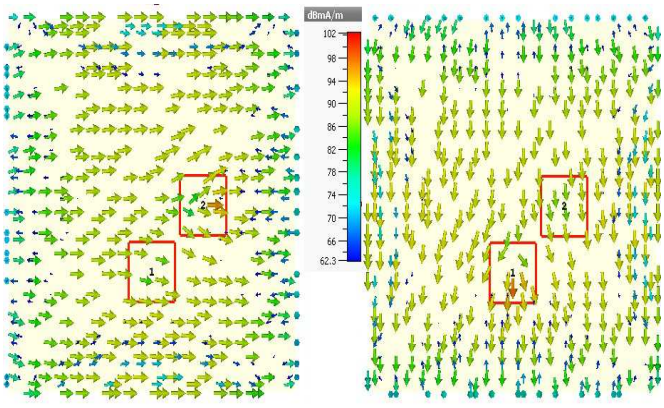

Figure 9. Surface current of initial antenna with dual coaxial feeds

4. ANTENNA WITH AIR-GAP BETWEEN SUBSTRATE AND GROUND

Figure 10 depicts a coaxially feed patch with length L and width W, designed on a FR4 substrate with an air gap (h2) between the ground plane and the substrate. The coaxial feed location (x, y) from the patch Centre determines the excitation of the TM modes, which launches the electric and magnetic fields along the suitable orthogonal axes for dual polarization. The extra linear dimensions L and W are used to account for the fringing of the electric fields at the radiating and non-radiating edges of the rectangular patch. The top layer is the substrate, which has a thickness of h1 and a relative permittivity of $\varepsilon_r(4.3)$, while the bottom layer is the air gap, which has a thickness of h2 and a relative permittivity of ε_o (1). The modified relative permittivity as given in [18].

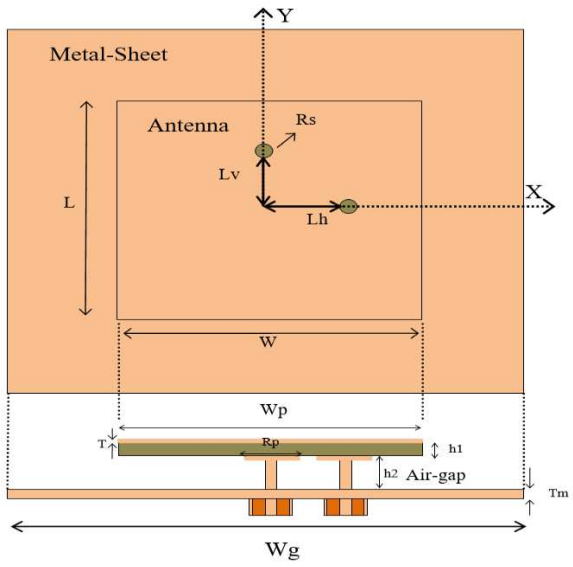

Figure 10. Proposed antenna with air-gap

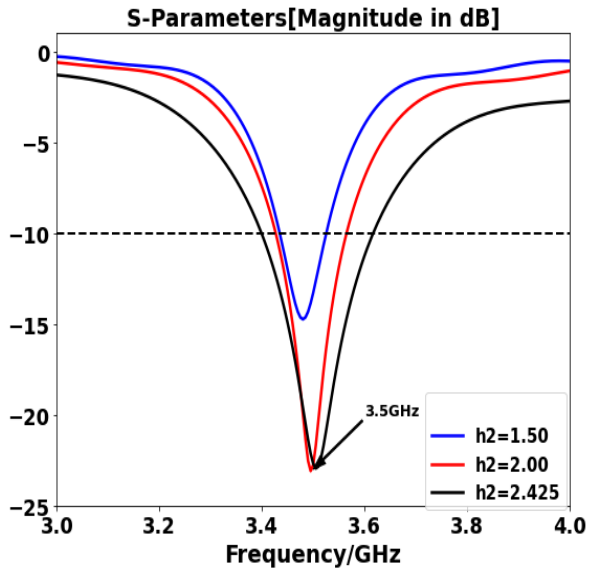

Figure 11. S11 Plot with air-gap height optimization

$$\varepsilon_{re} = \frac{\varepsilon_r(1+{}^{h_2}/_{h_1})}{(1+\varepsilon_r{}^{h_2}/_{h_1})} \tag{9}$$

Where, ε_{re} is the equivalent permittivity of the two-layer dielectric medium (see in figure 10) having total thickness h=h1+h2. As the air gap width h2 increases, ε_{re} decreases and the resonant frequency increases.

4.1. Bandwidth Enhancement by Air-gap

The advantage of this design is that it increases the microstrip antenna's height rather than its lateral dimension. The basic concept of microstrip antenna bandwidth improvement is to use a low effective permittivity of dielectric substrate and increase the thickness of the microstrip antenna by introducing an air-gap between the ground plane and the substrate, as shown in figure 10. Using this method, the equivalent permittivity of the microstrip antenna is reduced by increasing the thickness of the antenna. As a result, while increasing the bandwidth of a microstrip antenna, the effective permittivity of the two-layer microstrip antenna is an important parameter to consider. The equations (10) used in this design is as follows: [19]

$$BW(\%) = \left(3.77\left(\frac{\varepsilon_r-1}{\varepsilon_r^2}\right)\frac{W}{L}\frac{h}{\lambda}\right) * 100 \tag{10}$$

The S11 plot shown in figure 11 with air-gap height optimization demonstrates that increasing the height of the air-gap increases the resonance frequency due to a decrease in the effective dielectric contact value.

4.2. Gain enhancement by air gap

The gain of antenna also increases by using technique. When the air gap are varies from h2=1.50 mm until 2.42 mm thickness the gain is increases as shown in figure 12 at h2=2.425mm gain is 8.54 dBi approx. Finally, a 2.42 mm (h2) air gap is introduced to the initial antenna to increase gain and bandwidth.

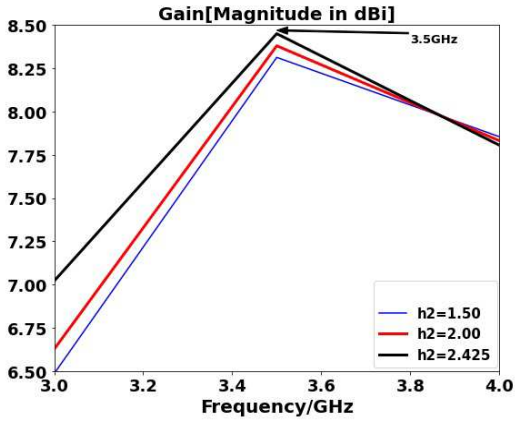

Figure 12. Gain plot with air-gap height optimization

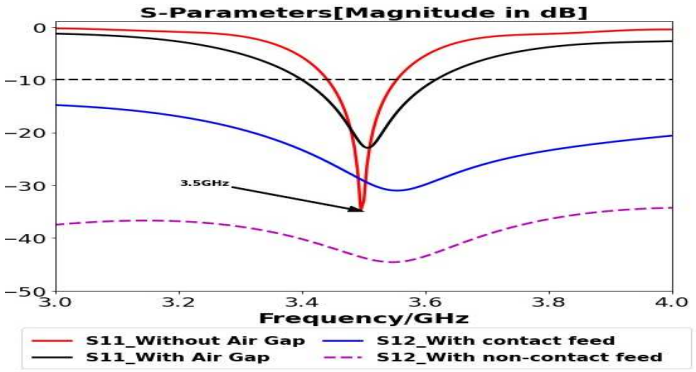

Figure 13. S11/S12 plot with contact and without non-contact feed antenna

4.3. Isolation/mutual coupling improvement with non-contact feed

The non-contact feed consists of circular aperture at top of antenna and circular metal plate at bottom of antenna, which is connect by coaxial inner conductor as shown in figure 10. So coaxial feed conductor is not direct contact to patch of antenna, it provides conducting current isolation between coaxial feed and patch part of antenna. Power is supply to antenna through electromagnetic coupling and the impedance matching is depends on radius of circular aperture and circular plate on antenna part. Figure 13 shows minimum mutual coupling (S12 parameter) between antenna ports for initial dual polarized antenna and air-gap non-contact dual polarized antenna as shown approx. -40dB coupling at 3.5Ghz.

5. WITH AIR-GAP AND WITHOUT AIR-GAP BASED ANTENNA PERFORMANCE COMPARISON

The air-gap and without air-gap with dual polarized antenna performance comparisons are discussed in this section. The bandwidth comparison is shown in figure 13 by S11 parameters. In this figure S11 red line shows the antenna without air-gap and black line shows the antenna with air-gap . So the desired bandwidth for sub-6 band 5G application is enhance by this method. Similar for gain and total efficicny are increased by using inserting air-gap between antenna as shown in figure 14 and 15 respectively.

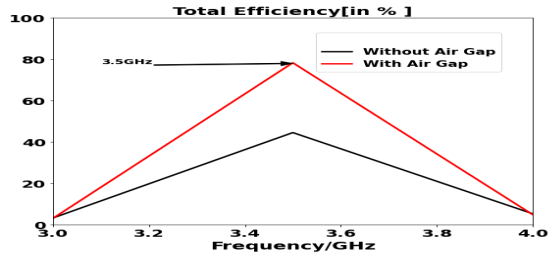

Figure 14. Total efficiency plot with air-gap height optimization

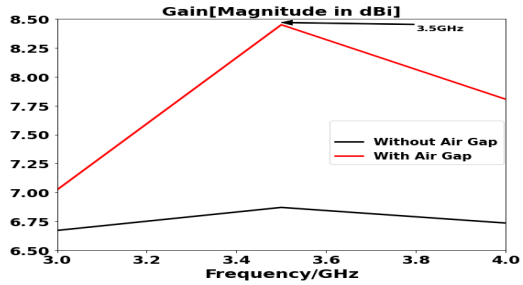

Figure 15. Gain plot with air-gap height optimization

6. PROPOSED 2*2 MIMO ANTENNA DESIGN

Figure 16, illustrated the detailed structure of proposed 2x2 MIMO antenna with air-gap between substrate and ground plane for sub-6 5G applications. The overall geometry of the proposed MIMO antenna is 120*120*5.17mm^3, and it printed on of a FR4 dielectric substrate (relative permittivity 4.4 and loss tangent 0.025.) with 1.6 mm height. Table 1 shows the parameters values of proposed MIMO antenna. The ground plane of MIMO antenna is 120*120*0.5 mm3. Each antenna element of MIMO systems are radiated by 50 Ω coaxial feed for dual polarization, so total 8-ports are required to operate 2x2 MIMO antenna. The scattering parameters of MIMO antenna are shown in figure 18, in this plot S11, S22, S33, S44, S55, S66, S77, and S88 shows for all 8-ports and resonate at 3.5 GHz from 3.4 to 3.6 GHz range for sub-6 5G desire bandwidth. Figure 19 shows mutual coupling parameters in terms of S21, S31, S41, S51, S61, S71, S81, and S81 between antenna ports and corresponding radiation pattern of each antenna elements are shown in figure 17. The isolation for MIMO is below 40dB at 3.5 GHz. Figure 20 and 21 shows electric field distribution of horizontal and vertical polarization respectively of each antenna elements in MIMO system.

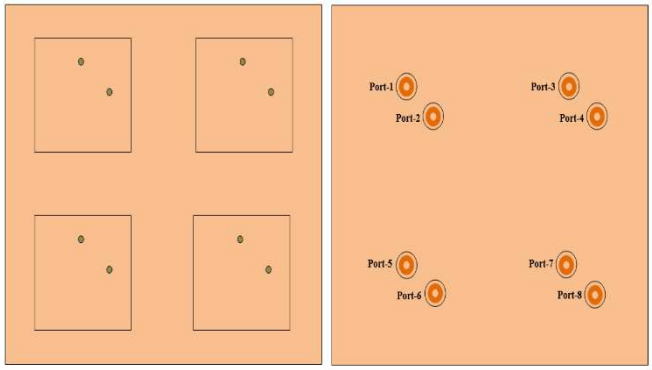

(a) (b)

Figure 16. 2x2 MIMO antenna with air-gap (a) top view, (b) bottom view

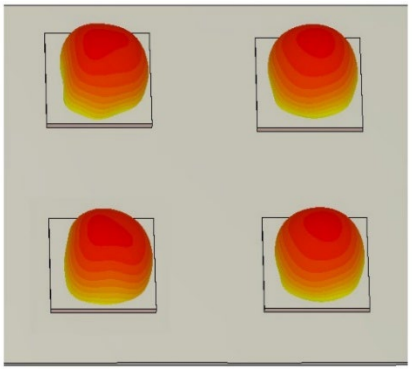

Figure 17. Radiation pattern of antenna with air-gap

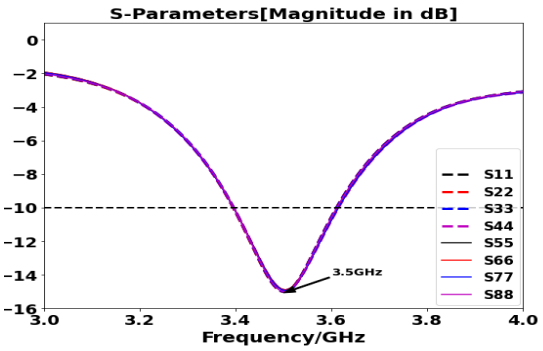

Figure 18. Scattering parameters of MIMO antenna

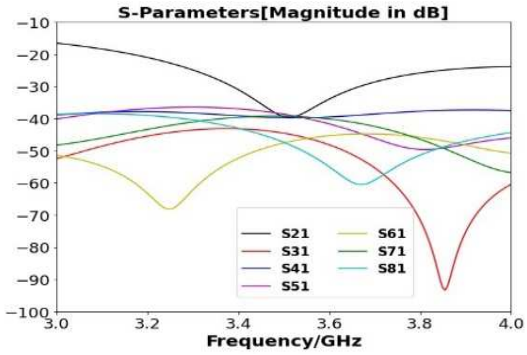

Figure 19. Mutual coupling parameters of MIMO antenna

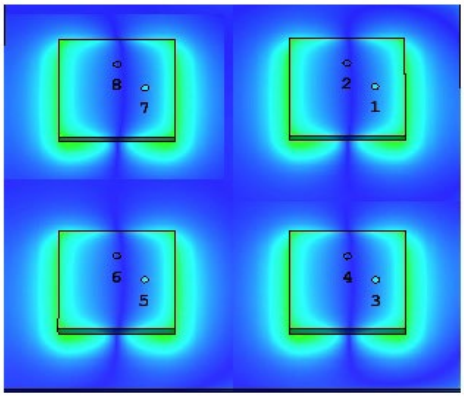

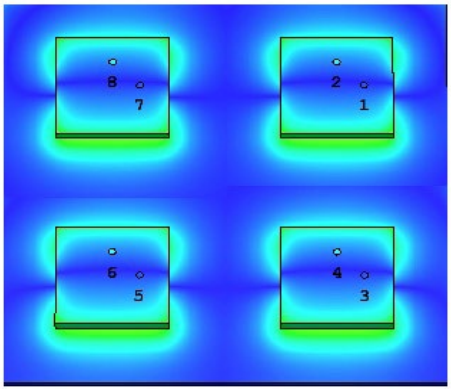

Figure 20. Electric field distribution of horizontal polarization

Figure 21. Electric field distribution of vertical polarization

TABLE 1. Dimensions of the proposed dual polarized MIMO antenna.

Parameters	Values (mm)	Parameters	Values (mm)
Lg	120	Lh	8.03
Wg	120	T	0.035
L	31.80	Tm	0.5
W	31.80	h1	1.6
Lv	8.03	h2	2.425
Rp	4	Rs	1

7.1 Diversity Performance of MIMO antenna

Isolation and radiation patterns aren't the only factors to consider when evaluating a MIMO antenna's performance. MIMO antenna performance is heavily influenced by diversity performance. The performance of diversity is described in terms of ECC (envelope correlation coefficients), DG (Diversity Gain), and CCL (Channel capacity loss) in this section.

7.1.1 Envelope correlation coefficients (ECCs)

Equation 11 is used to compute the envelope correlation coefficients (ECCs) of the proposed MIMO antenna from the simulated scattering parameters. Figure 22 depicts the simulated ECC characteristic of 2*2 MIMO systems, which reveals that the ECCs are very modest (i.e., < 0.001) over the entire bandwidth [4].

$$ECC=\frac{|S_{11}*S_{12}+S_{21}*S_{22}|^2}{(1-|S_{11}|^2-|S_{21}|^2)(1-|S_{22}|^2-|S_{12}|^2)} \quad (11)$$

The antenna's reflection and transmission coefficients are S11/S22 and S21/S12, respectively.

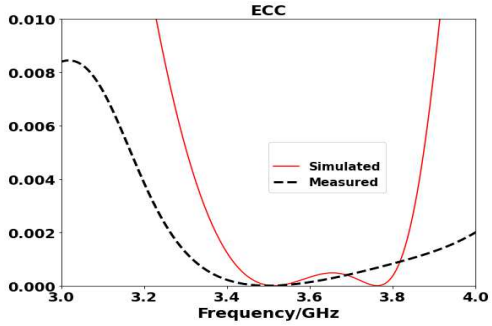

Figure 22. ECC plot for simulated and measured

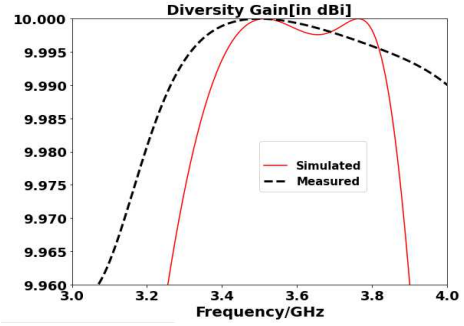

Figure 23. Diversity gain plot for simulated and measured

7.1.2 Diversity Gain (DG)

The signal-to-noise ratio enhancement as compared to a single antenna is referred to as diversity gain. In [20], DG is calculated and plotted using (12) and plotted in figure 23. The computed DG values from simulated and measured ECC are nearly 10 dB, as shown in the plot.

$$DG = 10\sqrt{1 - ECC^2} \quad (12)$$

7.1.3 Channel Capacity Loss (CCL)

The capacity of a MIMO system increases as the number of antennas increases. However, due of the addition of a correlation factor between the MIMO antennas parts, channel capacity losses increase as well. The loss of channel capacity caused by the correlation of two antenna elements is referred to as channel capacity loss. CCL with a lower value is better. To achieve superior MIMO diversity performance, the CCL value can be calculated using equation (13), and it must be less than 0.1(bits/s/Hz) [21].

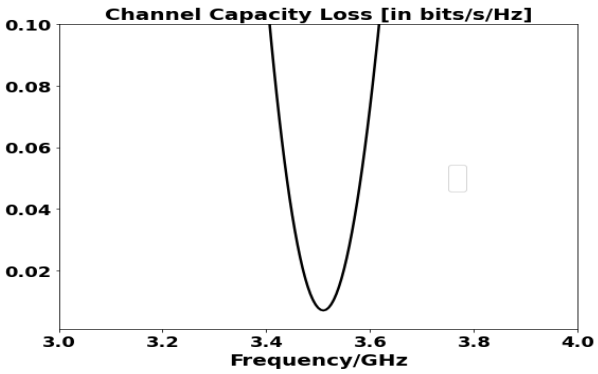

Figure 24. Channel Capacity Loss plot for MIMO antenna

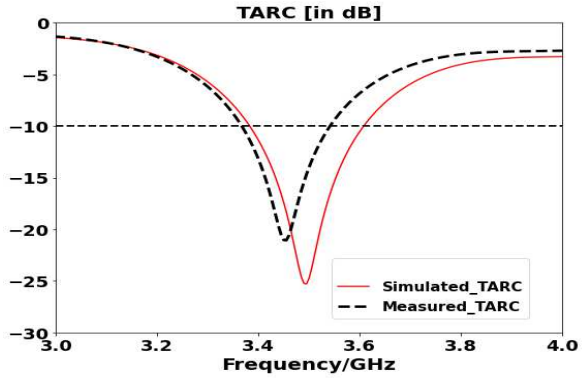

Figure 25. Simulated and Measured TARC plot of MIMO antenna

$$CCL = -log_2[\det(\psi^R)] \quad (13)$$

$\psi^R = \begin{bmatrix} \varphi_{11} & \varphi_{12} \\ \varphi_{21} & \varphi_{22} \end{bmatrix}$, and

$$\varphi_{11} = 1 - (|S_{11}|^2 + |S_{12}|^2)$$
$$\varphi_{22} = 1 - (|S_{22}|^2 + |S_{21}|^2)$$
$$\varphi_{12} = S_{11}^* S_{12} + S_{21}^* S_{12}$$
$$\varphi_{21} = S_{22}^* S_{21} + S_{12}^* S_{21}$$

Figure 24 illustrates the calculated channel capacity loss for the full operating band, which is significantly below 0.1(bits/s/Hz). As a result, the proposed antenna performs exceptionally well in MIMO diversity.

7.1.3 Total active reflection coefficient (TARC)

The return loss of the entire MIMO proposed antenna is known as the total active reflection coefficient, or TARC. Equation can be used to determine it (14). The overall active reflection coefficient of the proposed MIMO antenna was simulated and tested, as shown in figure 25. The computed TARC findings are extremely low across the whole band of interest, as seen in the figures.

$$TARC = -\sqrt{\frac{(S_{11}+S_{12})^2+(S_{21}+S_{22})^2}{2}} \text{ [22]} \quad (14)$$

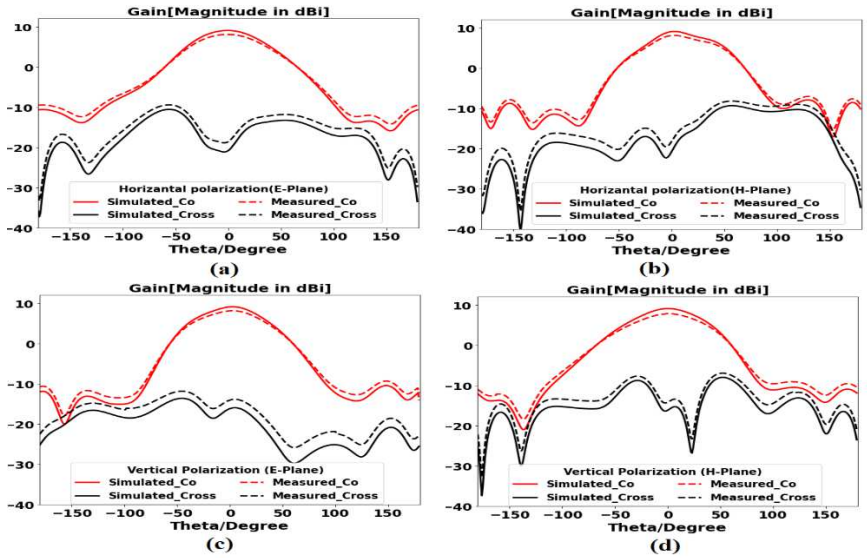

Figure 26. Gain Plots of MIMO antenna (a) horizontal Pol. of E-Plane, (b) horizontal Pol. of H-Plane, (c) Vertical Pol. of E-Plane, (d) Vertical Pol. of H-Plane

8. FABRICATION AND MEASUREMENT ANALYSIS

The 2x2 MIMO antenna were fabricated and examined its properties. Figure 27 (a,b)depicts both top and bottom views of the prototype. The MIMO antenna has an overall diameter of 120 120 5.17 mm3 and is made of a cheap FR4 dielectric. As shown, the MIMO antenna achieves excellent S parameters in the necessary frequency range, with appropriate impedance bandwidth and low mutual coupling characteristic, as well as desirable gain in the broadside direction as shown in figure 26. Errors in the fabrication, feeding, and experimentation procedures cause certain variances from the measurements.

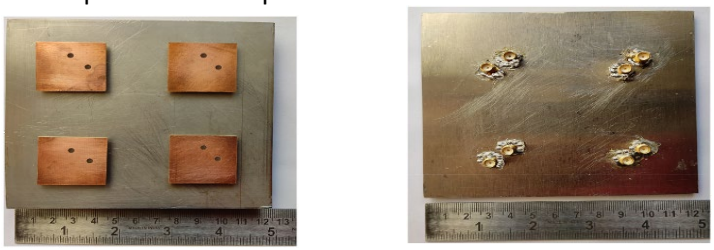

(a) (b)

Figure 27. Photograph of the fabricated MIMO antenna hardware (a) Top view, (b) bottom view

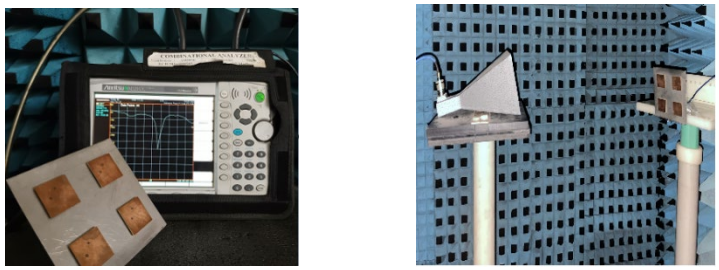

(a) (b)

Figure 28. Photograph of measured MIMO antenna hardware set-up (a) Scattering parameters, (b) Anechoic chamber for radiation patterns measurement

Table 2: Previous antennas are compared to the proposed antenna.

Ref	Frequency Band (GHz)	Gain(dBi)	Circuit Complexity)	Port Isolation	ECC	Total efficiency	Size(mm^3)	(Material)
2(2022)	3.4 - 3.6	8.26	M	32	0.020	86-88	40*40*21.42	FR4
4(2021)	1.55-6	NA	M	16	0.500	84	129.5*129.5*28.2	R04003C
5(2021)	2.35-4.25	8.34	M	28.65	0.027	81.8	125.2*125.2*18	FR4
7(2017)	4.9-6	8.7	M	20	0.300	80-85	30*30*13	RT5880
12(2021)	3.45-3.55	9.41	M	21	0.119		74*74*1.524	RO4350B
10(2021)	3.1-5	7.5	H	30	NA	82.6%	32 32 33.8	FR4
11(2020)	3.5-4.9	2.26	H	20	NA	90	60*60*19.5	FR4
6(2020)	3.2-3.9	5.2	M	40	0.0045	NA	31 × 31 × 14	FR4
8(2021)	1.32-2.82	8.4	H	30	NA	NA	110*110*38.4	FR4
9(2021)	3.14-3.92	8.6	M	28	NA	NA	110*110*11.1	FR4
PROPOSED	3.4-3.6	9.19	S	40	0.001	87	60*60*5.17	FR4

S-Simple, M-moderate, H-high

8. CONCLUSION

A 2*2 MIMO antenna system for 3.4–3.6 GHz is designed for sub-6, 5G indoor base station applications. The use of non-contact feed reduces mutual interaction between the antenna's ports. The isolation has been enhanced and is now less than 40 dB over the whole operating range. Four separate unidirectional radiation patterns with excellent efficiency are provided by the design. The MIMO antenna is designed on a FR4 substrate, which is readily available, affordable, and frequently utilized. CST Studio Suite, an EM full-wave software, was used to design the proposed antenna. A full analysis of the antenna design, non-contact feed, and other design factors is presented. The proposed antenna prototype is fabricated to validate the simulated results with measurement results. When the simulation and measurement results are compared, they show that they are in good agreement. The effects of antenna isolation on the MIMO system are also investigated. The proposed system's ECC and Diversity Gain (DG) are determined to be 0.001 and 10 dBi, respectively. The channel capacity loss (CCL) for the whole operating bandwidth is less than 0.1 bits/s/Hz, and the vertical and horizontal gain is around 9.19dBi.

REFERENCES

[1] Le Thi, Cam Ha, et al. "Design of compact broadband dual-polarized antenna for 5G applications." *International Journal of RF and Microwave Computer-Aided Engineering* 31.5 (2021): e22615.

[2] Bellary, Anudeep, Krishnamoorthy Kandasamy, and Patnam Hanumantha Rao. "Analysis of Wave Propagation Models with Radio Network Planning using Dual Polarized MIMO Antenna for 5G Base Station Applications." IEEE Access (2022).

[3] Zhou, Weiwei, Zhiqun Cheng, and Y. Jay Guo. "A Dual-Polarized Patch Antenna With Electric and Magnetic Coupling Feed for 5G Base Stations." 2020 IEEE 5th International Conference on Integrated Circuits and Microsystems (ICICM). IEEE, 2020.

[4] Molins-Benlliure, Jaime, et al. "Four-Port Wide-Band Cavity-Backed Antenna With Isolating X-Shaped Block for Sub-6 GHz 5G Indoor Base Stations." IEEE Access 9 (2021): 80535-80545.

[5] Yang, Shuhui, et al. "Wideband Gain Enhancement of an AMC Cavity-Backed Dual-Polarized Antenna." IEEE Transactions on Vehicular Technology 70.12 (2021): 12703-12712.

[6] Li, Mengting, et al. "Dual-polarized broadband base station antenna backed with dielectric cavity for 5G communications." *IEEE Antennas and Wireless Propagation Letters* 18.10 (2019): 2051-2055.

[7] Komandla, Mohana Vamshi, Ghanshyam Mishra, and Satish K. Sharma. "Investigations on dual slant polarized cavity-backed massive MIMO antenna panel with beamforming." IEEE Transactions on Antennas and Propagation 65.12 (2017): 6794-6799.

[8] Wu, Chao, et al. "Bandwidth Enhancement of Broadband Dual-Polarized Dipole Antenna for 5G Base Station." 2021 IEEE 4th International Conference on Electronics Technology (ICET). IEEE, 2021.

[9] Çiydem, M. E. H. M. E. T. "A Low-Profile Dual-Polarized Antenna with High Isolation and High Front-to-Back Ratio for 5G Base Stations." The Applied Computational Electromagnetics Society Journal (ACES) (2021): 1229-1236.

[10] Dual-Polarized Highly Folded Bowtie Antenna with Slotted Self-Grounded Structure for Sub-6 GHz 5G Applications.

[11] Yang, Shuming, et al. "Decoupling of Wideband Dual-Polarized Base Station Antennas for Sub-6 GHz Applications." 2020 International Conference on Microwave and Millimeter Wave Technology (ICMMT). IEEE, 2020.

[12] Al-Tarifi, Monjed A., Mohammad S. Sharawi, and Atif Shamim. "Massive MIMO antenna system for 5G base stations with directive ports and switched beamsteering capabilities." IET Microwaves, Antennas & Propagation 12.10 (2018): 1709-1718.

[13] Lohar, Fateh L., et al. "T-Shaped Tri-Band Antenna Based on Characteristic Mode Analysis for Satellite Applications." Progress In Electromagnetics Research C 115 (2021): 65-81.

[14] Lohar, Fateh Lal, et al. "Design of circularly polarized irnss receiver antenna using characteristic mode analysis." 2019 IEEE Indian Conference on Antennas and Propogation (InCAP). IEEE, 2019.

[15] Suyan, Nitin Kumar, et al. "Design of Compact Size Tri-Band Stacked Patch Antenna for GPS and IRNSS Applications." Congress on Intelligent Systems. Springer, Singapore, 2020.

[16] Singh, Jaget, Fateh Lal Lohar, and B. S. Sohi. "Design of dual band millimeter wave antenna using SIW material for 5G cellular network applications." Materials Today: Proceedings 45 (2021): 5405-5409.
[17] Balanis, Constantine A. *Antenna theory: analysis and design*. John wiley & sons, 2015.

[18] Chattopadhyay, Sudipta, et al. "Rectangular microstrips with variable air gap and varying aspect ratio: improved formulations and experiments." Microwave and Optical Technology Letters 51.1 (2009): 169-173.

[19] Yoharaaj, D., Raja Syamsul Azmir, and Alyani Ismail. "A new approach for bandwidth enhancement technique in microstrip antenna for wireless applications." *2006 International RF and Microwave Conference*. IEEE, 2006.

[20] Islam, Sk Nurul, and Santanu Das. "Isosceles Triangular Resonator Based Compact Triple Band Quad Element Multi Terminal Antenna." Radioengineering 29.1 (2020).

[21] Khan, Awais, et al. "Mutual coupling reduction using ground stub and EBG in a compact wideband MIMO-antenna." IEEE access 9 (2021): 40972-40979.

[22] Ojaroudi Parchin, Naser, et al. "Mobile-phone antenna array with diamond-ring slot elements for 5G massive MIMO systems." *Electronics* 8.5 (2019): 521.